Journal Pre-proof

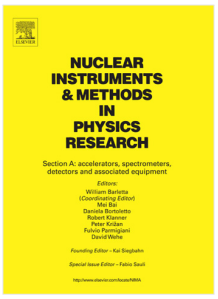

Overview of planned upgrade to the secondary spectrometer of TOSCA

Adrien Perrichon, Claudio Bovo, Stewart F. Parker, Davide Raspino, Jeff Armstrong, Victoria García Sakai

PII: S0168-9002(22)01191-3
DOI: https://doi.org/10.1016/j.nima.2022.167899
Reference: NIMA 167899

To appear in: *Nuclear Inst. and Methods in Physics Research, A*

Received date : 14 September 2022
Revised date : 24 October 2022
Accepted date : 27 November 2022

Please cite this article as: A. Perrichon, C. Bovo, S.F. Parker et al., Overview of planned upgrade to the secondary spectrometer of TOSCA, *Nuclear Inst. and Methods in Physics Research, A* (2022), doi: https://doi.org/10.1016/j.nima.2022.167899.

Overview of Planned Upgrade to the Secondary Spectrometer of TOSCA

Adrien Perrichon[a,*], Claudio Bovo[a], Stewart F. Parker[a], Davide Raspino[a], Jeff Armstrong[a], Victoria García Sakai[a]

[a] *ISIS Facility, Rutherford Appleton Laboratory, Chilton, Didcot, Oxfordshire OX11 0QX, United Kingdom*

Abstract

We describe a proposed upgrade to the indirect-geometry broad-band chemical spectrometer TOSCA at the ISIS Neutron and Muon Source, UK. By replacing the secondary spectrometer of the instrument, we expect a gain in detected intensity of an order of magnitude, improved spectral resolution over the entire energy range of the instrument and an improved signal-to-noise ratio. The new secondary spectrometer consists of 14 analyser modules, each constituted of a large, curved pyrolytic graphite analyser, a beryllium filter and a position-sensitive detector system. We present the prospective design and expected performance of the new analyser module as calculated from ray-tracing simulations. The improved performance will develop the instrument capabilities to tackle new and challenging experiments and ensure that TOSCA remains highly competitive in the years to come.

Key words: TOSCA, indirect-geometry neutron spectrometer, ray-tracing simulations, neutron spectroscopy

*Corresponding author
Email address: adrien.perrichon@stfc.ac.uk (Adrien Perrichon)

Introduction

TOSCA is a high-resolution, broad-band, chemical spectrometer operated at the ISIS Neutron and Muon Source, UK. It is optimised for the study of molecular vibrations and can thus be considered as a neutron analogue of infrared and Raman spectrometers. TOSCA is requested in many fields of science, such as catalysis in zeolites [1, 2] and metal–organic frameworks [3], energy materials for hydrogen storage [4, 5] and protonics [6], materials discovery of, for example, novel oxyhydrides [7] and polymers [8], as well as biological and medical sciences [9–11].

TOSCA is an indirect-geometry instrument where the neutron final energy is selected by Bragg reflection from the (002) plane of a flat pyrolytic graphite (PG) analyser, and where the neutron incident energy is determined by measuring the time-of-flight (TOF). Its design is very similar to the VISION spectrometer [12] at the Spallation Neutron Source (SNS, Oak Ridge, TN, USA), but VISION has large, curved, image-focusing PG analysers with position-sensitive detectors (PSD), which give a larger solid angle coverage of the analyser and thus an increased detected intensity, at the price of only a minor degradation of the spectral resolution. As TOSCA once inspired VISION's design, VISION is now itself inspiring the TOSCA upgrade and the design of the VESPA spectrometer [13, 14] to be built at the European Spallation Source (ESS, Lund, Sweden).

At high energy transfer, in the so-called fingerprint region of $\hbar\omega = 50$–185 meV (400–1500 cm^{-1}), TOSCA exhibits excellent spectral resolution of $\sim$1.5% of the incident energy, which is achieved by the time- and energy-focusing geometry of its secondary spectrometer [15, 16]. The spectral reso-

lution of TOSCA has been studied in detail in ref. [17, 18], with an analytical method which identified the critical contributions to the resolution and with neutron ray-tracing simulations which serve as a reference with which to compare any future simulations.

In 2017, a high-m supermirror guide was installed on TOSCA, which has dramatically increased the incident flux on the sample, by a factor 10 at high energy transfer and up to 80 at the elastic line, while maintaining the excellent spectral resolution and signal-to-noise ratio (SNR) of the instrument [19, 20]. To fully capitalise on this successful upgrade and to further increase the detected intensity and SNR, an upgrade of the secondary spectrometer is needed.

We present here an overview of the design and performance of the proposed upgrade of the TOSCA secondary spectrometer. The entire secondary spectrometer will be replaced and a new set of large, curved PG analysers, beryllium (Be) filters and PSDs will be installed. The design, dimensions and position of each component has been optimised with neutron ray-tracing simulations. Compared to previous iterations of the design [21, 22], the spatial arrangement of the analyser modules is staggered and the optical focal point of the curved analyser is located at a distance behind the detector, which significantly improves the instrument performance. A gain factor in detected intensity of a least 10 is expected over the current instrument, independent of the energy transfer. This results from the increased solid angle coverage, increased transmission of analysed neutrons through the filter and increased neutron detection efficiency. The predicted spectral resolution improves for all energy transfers over the current instrument, with a value close to $\sim$1.1%

of the incident energy at high energy transfer, which can be further enhanced to as low as 0.8% by software masking of the PSD array. Furthermore, the performance of the beryllium filter in eliminating high energy neutrons has been improved by a factor of 10 which, together with a careful shielding of the secondary and a judicious choice of the analyser construction materials, should improve the SNR and thus the sensitivity and detection and quantitation limits of the instrument.

The overall improvement in performance is crucial to develop the instrument capabilities in measuring samples that are challenging to produce in large quantities, for instance biological samples. The improvement of the resolution and especially the SNR will improve the quantitation limit of the instrument, which is currently estimated to be $\sim$430 μmol of elemental hydrogen analytes in ZrH_2 [23]. The gain in intensity will shorten measurement times and allow milligram-size samples to be measured routinely. Besides reducing the sample size, the performance gains will also benefit studies of non-hydrogenous materials, such as battery materials, or CO_x, SO_x, NO_x and N_2 adsorbed on catalysts, as well as deuteration studies which allow the highlighting of modes within a given molecular group [24].

Design process

General concept

The careful modelling of TOSCA has unveiled four ways to increase the detected intensity [17, 18, 22]. The first, and most important, is to increase the solid angle coverage of the PG analyser by using curved analysers as demonstrated by VISION, from the current coverage of about 1 sr to the

maximum coverage in the range 6.0–6.3 sr allowed by the space constraints. The second is to improve the transmission of low-energy analysed neutrons through the Be filter, from the current transmission of ∼50% to at least 75–80%, thus achieving a gain factor of 1.5–1.6. The third is to further improve the efficiency of the detector system, from the current value of about ∼81% to a value as close as possible the upper limit in efficiency of the high pressure ^{3}He tubes, considered here to be about 90%, thus a gain factor of about 1.1. The fourth, and more minor, contribution comes from capturing the entire neutron image at the detector position, which is not the case for the current TOSCA which captures only about 95% of the neutron image. These four contributions together, lead to an expected increase in detected intensity in the range of 10.4 to 11.6.

To a first approximation, the background signal measured by the TOSCA detectors originates exclusively from the secondary spectrometer. The background originates from stray low-energy neutrons scattered through the filter, for instance neutrons elastically scattered by Al from the analyser back plate, and from high-energy neutrons that are either directly transmitted through the filter or elastically scattered through it via multiple scattering (thermal leakage [25]). These two sources of background are proportional to the number of neutrons reaching the beryllium filter, thus we can expect an increase of the background signal matching the increase in solid angle, hence a nearly constant signal-to-noise ratio (SNR). However, the upgrade of the secondary provides the opportunity to increase the SNR by improving the filtering performance of the Be filter for high energy neutrons. This is achieved by increasing the thickness of the Be filter, as well as by reduc-

ing the spacing between the neutron absorbing blades built-in to the filter, which decreases both the direct transmission of high energy neutrons and their thermal leakage.

Achieving a solid angle coverage of at least 6 sr requires a large and curved PG analyser with image-focusing capabilities. At otherwise strictly identical instrument components, using a curved PG analyser leads to a degradation of the energy resolution of the instrument at high energy transfer. This is due to a departure from the ideal time- and energy-focusing geometry enabled by the flat PG analyser. The degradation of this contribution from the PG analyser to the resolution can be minimised by carefully optimising the surface curvature of the analyser and the orientation of the individual PG tiles, in a way that restores a degree of time- and energy-focusing. The best solution found here requires focusing neutrons at a distance behind the detector plane, which leads to a large image on the detector compared to the point-image achieved on VISION. As the secondary TOF is not strictly uniform across the image, and given the gradient of neutron final energy, the use of PSDs is required. Note that, besides the contribution from the PG analyser, a significant contribution to the spectral resolution of the current TOSCA is due to the large intrinsic time resolution of the squashed ^{3}He tubes used. By using state-of-the-art high pressure cylindrical ^{3}He tubes, this contribution can be significantly reduced, which more than compensates for the degradation of the resolution from the curved optics. It follows that the spectral resolution of the upgraded instrument will improve with respect to the current one.

In designing the new secondary spectrometer, a major consideration is

that the primary spectrometer remains unchanged, which fixes the sample position at its current position. Additionally, given the proximity to other instruments and the limited size of the instrument's pit, the footprint of the upgraded secondary must be identical to, or only marginally larger than, the current footprint of the instrument. These spatial constraints spawn the main technical challenges of the upgrade: how to fit large PG analysers, large cryo-cooled Be filters, large PSDs and associated cables and electronics, into an extremely crowded vacuum vessel, while achieving the target performance gain.

Neutron ray-tracing simulations

The numerical simulations of the instrument were performed with the Monte Carlo ray-tracing package McStas version 2.7.1 [26–28], operated with an in-house Matlab code. Detailed information on the choice of the McStas components used to describe each element of the instrument are reported elsewhere [17, 18].

Neutron rays reaching the detector position are monitored and stored as individual rays in "event mode". Post-processing of the neutron rays is performed in Matlab to include the effect of the Be filter collimation, propagation of the neutron inside the detector and binning into histograms based on the PSD's spatial resolution. As shown hereafter, because of the complex shape of the Be filter, the analytical transmission of analysed neutrons through the neutron absorbing blades of the filter is not known *a priori*. Instead of using an analytical model, the collimation is accurately accounted for by a Monte Carlo calculation that checks, for each neutron ray, the intercept condition with the neutron absorbing blades of the Be filter. The neutron propaga-

tion in the detector considers the detector geometry, which is an array of cylindrical tubes at 20 bar ^{3}He pressure, which gives a truncated exponential decay for the capture profile. The data reduction that converts the simulated spectra from TOF to energy transfer is performed for each pixel of the PSD independently. The reduced spectra are then summed and curvefit to obtain the simulated spectral resolution.

Note that the simulations are performed for the standard sample size of $40 \times 40 \times 1$ mm^3 and that the contributions of the PG tile thickness and detector thickness on the secondary TOF are accounted for. While this degree of detail is usually not necessary in ray-tracing simulations for most instruments, it is critical to correctly estimate the spectral resolution of TOSCA at high energy transfer. Indeed, at high energy transfer the secondary and primary TOFs become comparable, and the uncertainty in the secondary TOF becomes a major contribution to the resolution [17, 18].

Design of the assembly

The assembly is the spatial arrangement of the PG analysers, beryllium filters and detectors inside the secondary spectrometer tank. The assembly of the current TOSCA, as well as that of VISION, can be considered as "back-to-back", with symmetric forward and backward scattering analyser modules, with the detector banks of the backward and forward modules sitting back-to-back, as illustrated in Fig. 1(a). The choice of the assembly contributes to the intensity gain, as the maximum solid angle is defined by the limits in polar angle (rotation around the instrument axis) and azimuthal angle (angle from the instrument axis) of the analyser.

The assembly also contributes to the achievable spectral resolution in two

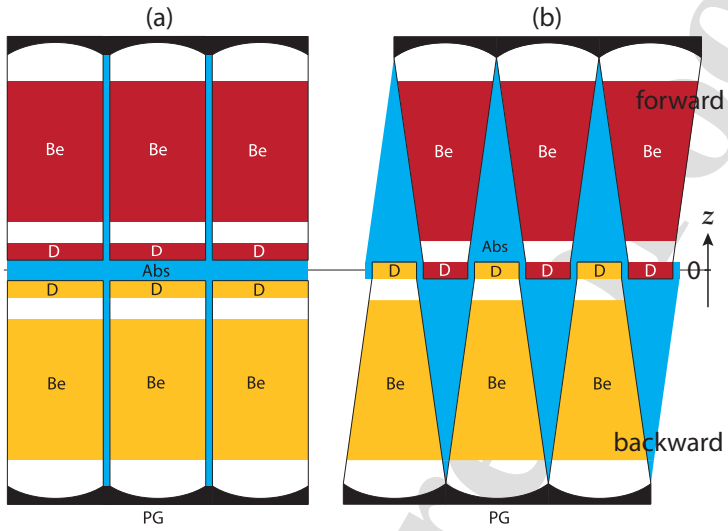

Figure 1: Scheme of (a) the back-to-back and (b) the staggered assemblies. Forward banks in red, backward banks in yellow, PG analyser in black, beryllium filters (Be), detectors (D) and neutron absorbing material in blue (Abs). Not to scale.

aspects. The first aspect is the distance between the detector plane and the sample plane, due to the detector thickness and need to fit neutron absorbing materials between the backward and forward banks to avoid crosstalk. This offset brings the geometry slightly out of the perfectly time- and energy-focusing condition for flat analysers, which is achieved at $z = 0$. While the position of the perfect time-focusing point can be offset to $z > 0$ with curved analysers, decreasing the secondary flight path necessarily increases the relative uncertainties in both the secondary flight path and secondary TOF, which degrades the resolution. The other aspect is a blurring effect from the degree of image-focusing imposed by the curved analysers, which is linked to the compression of the image from the large analyser to the

smaller detector area. Indeed, neutrons scattered from an extended area of the analyser will reach the same detector pixel. While the average secondary TOF can be made equal for all tiles with curved analysers, because of the finite dimensions of the tiles and the variation of their orientations across the analyser, there is still a mismatch between the gradients of secondary TOFs and final energies averaged out by the detector pixel. This problem is minimised in the current TOSCA as the neutron beam is diverging all the way through sample to detector, with an image at the detector position larger than the analyser dimensions.

Based on these two aspects, in order to improve the spectral resolution beyond the back-to-back assembly design, we can either limit the image focusing to the vertical direction and keep the analyser flat horizontally, which would lead to a continuous and radially tiled analyser, or stagger the backward and forward banks to bring all detectors to the same plane at $z = 0$, as illustrated in Fig.1(b). Either way, it is beneficial for the resolution to spread the image as much as possible on the available detector area, which minimises the blurring effect.

We selected the staggered assembly option as it minimises the cost of the upgrade, with only half the number of detectors required and smaller beryllium filters, while achieving the target performance. Furthermore, at equal beryllium filter thickness, the staggered assembly with curved analysers exhibits both a slightly higher solid angle and a better resolution than the back-to-back assembly. The best solution in terms of gain and resolution is to divide the analyser area into 14 arms, with 7 arms in backward and 7 arms in forward scattering positions, each with a polar angle coverage of

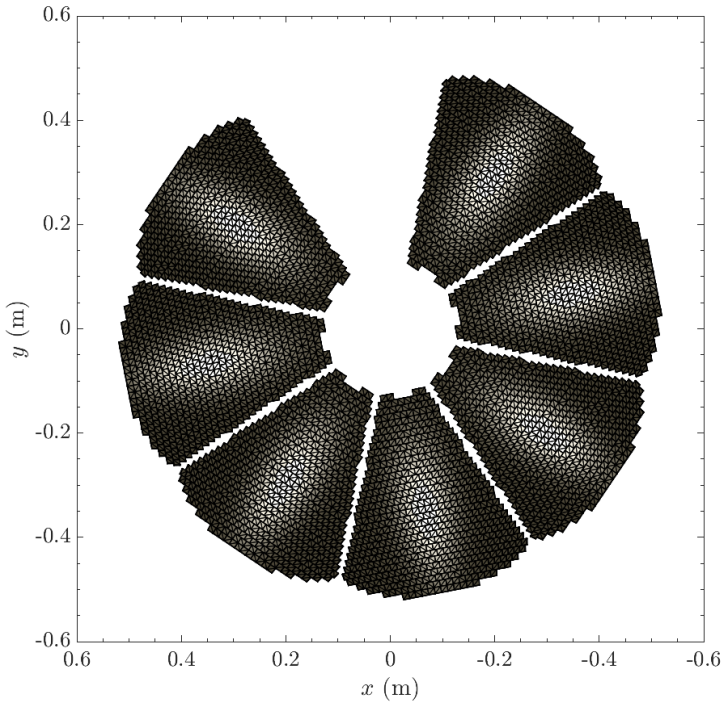

Figure 2: Layout of the PG analysers of the 7 backward banks, projected in the (x,y)-plane. Each grey rectangle represents a $12 \times 12 \times 2$ mm^3 PG tile. Each of the 14 analysers consists of ∼600 tiles, for a total of ∼8400 tiles covering an area of ∼1.2 m^2.

45° and azimuthal angle limits of 27.5° and 72°. This is illustrated for the backward bank in Fig. 2, and leads to an extremely large solid angle of 6.3 sr, which is to be compared with 1 sr for the current TOSCA, 2.5 sr [29] for the LAGRANGE spectrometer at the Institut Laue Langevin (ILL, Grenoble, France), and estimated at 3.6 sr for VISION and 5.2 sr [13] for VESPA.

Analyser construction strategy

After choosing the design of the assembly, which fixes the dimensions of the analyser and positions and dimensions of the detector area, the next step is to construct the analyser defined by the list of PG tile positions and orientations. Modelling work on the current TOSCA [17, 18] and VISION [12] instruments clearly evidences that it is the uncertainties in the secondary TOF which determine the spectral resolution in the fingerprint region and at high energy transfer. Conversely, the uncertainties in the secondary flight path mainly contribute to the resolution at the elastic line and at low energy transfer. The analyser should thus be constructed in a way that minimises the secondary TOF uncertainties and, if possible, the secondary flight path uncertainties.

Multiple strategies are available to construct the analyser. If the design aims for the highest degree of image focusing, as implemented on VISION, with ideally a spot image on the detector for which neutrons scattered on the entire analyser contribute, one should ensure that the mean secondary TOF of each tile constituting the analyser is strictly equal. Alternatively, in the case of a looser degree of image focusing, with the image spread to occupy the entire detector area, and because only a limited region of the analyser contributes to a specific detector pixel, a small and smooth gradient of secondary TOF across the analyser may be acceptable. In this second scenario, monitoring the PG tiles properties (secondary TOF, secondary flight path, final energy) is not enough and one needs to instead monitor the properties of the PSD pixels. In order to achieve this, the solution which provided the best results was a holistic approach where the entire analyser is constructed

and evaluated as one, by monitoring the achieved spectral resolution at the upper end of the fingerprint region at $\hbar\omega = 150$ meV.

The construction strategy of the analyser implemented here is as follows: PG tiles are placed on a 3D ellipsoid defined by two ellipses, for the vertical and horizontal curvatures, respectively. This requires 1 constrained parameter which is the instrument footprint, and 6 free parameters which are the focal point positions (FP) of the two ellipses (4 vertically and 2 horizontally). To minimise the secondary flight path uncertainties, the FPs are located near the sample and detector positions. The tiles are then tilted away from the surface tangent to face a point in space located either in the detector plane for a point image, or behind the detector to spread the image, which gives 3 additional free parameters (2 vertically and 1 horizontally). Fortunately, the vertical and horizontal profiles are uncorrelated, which simplifies the optimisation. By focusing the image at a distance behind the detector, thus having a spread image at the detector position, we minimise the blurring and we obtain a smooth gradient of secondary TOFs and secondary flight paths across the detector area, which is then resolved by the PSD. The best result leads to the analyser shown in Fig. 2, which is constituted of ∼600 tiles, thus a total of ∼8400 tiles for the 14 analysers, covering an area of ∼1.2 m^2.

Beryllium filter construction strategy

The beryllium filter is an assembly of beryllium wedges each separated by neutron absorbing blades. Its purpose is to improve the SNR by lowering the background in the detected signal. The filter achieves this aim by filtering-out higher-order scattering from the PG analyser, stray neutrons resulting from scattering by the sample environment and eliminates the direct line-of-sight

between sample and detector. The performance of the Be filter depends on the transmission of low-energy neutrons that are analysed by the PG analyser and on the transmission of high-energy neutrons scattered through the beryllium by thermal leakage. The transmission of both the low- and high-energy neutrons depends on the effective path length of beryllium seen by the neutrons, which is determined by the beryllium filter's shape and thickness. The transmission also depends on the spacing between the neutron absorbing blades, which on one hand sets the divergence cut-off of low energy neutrons (acting as a collimator), and on the other hand impacts the thermal leakage of high energy neutrons. A well-performing Be filter would ideally maximise the transmission of low-energy neutrons that are analysed by the PG analyser and minimise the transmission of high-energy neutrons that contribute to the background signal.

We have shown in ref. [17] that on TOSCA the transmission of analysed neutrons through the filter is 48±3%, which is due to the mismatch between the incoming diverging beam from the analyser and the horizontal linear collimation of the filter, which was retrofitted on the instrument by slicing the previously used Be monolith. To improve the transmission of low-energy neutrons, we need to align the neutron blades according to the incoming divergence. This can be done either on the horizontal divergence, which gives a radial collimator as implemented on VISION, or on the vertical divergence, which gives a more complex filter. The latter has two unique advantages. Collimating vertically allows a flat surface on the detector side, which enables the filter to be closer to the detector, thus allowing for a thicker filter.

The second advantage is linked to the shape and dimension of the filter,

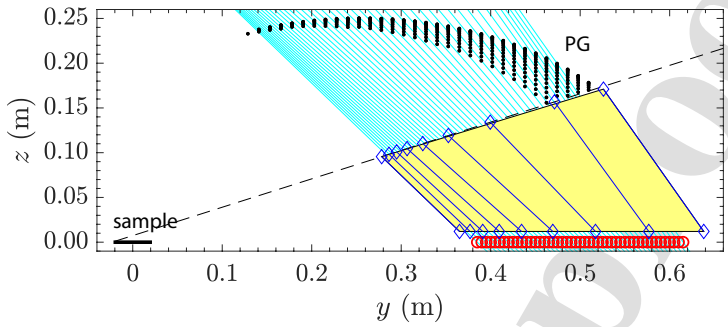

Figure 3: Scheme of the beryllium filter showing the 8 wedges of beryllium (yellow) separated by neutron absorbing material (blue lines). The shape of the filter is determined by the line-of-sight between the bottom of the sample and the top of the analyser (dashed black line) and the array of detectors (red markers). The gap between the beryllium backplate and the detector surface is set to 12 mm. The average incident vertical divergences for each detector pixel are shown by cyan lines.

which is limited by the line-of-sight from the sample to the uppermost tile of the analyser on one side and the detector on the other side, resulting in a triangular shape as illustrated in Fig. 3. As the path length of Be seen by the neutron varies along the height of the filter, so does the performance in filtering high energy neutrons if the neutrons absorbing blades were collimating horizontally. Collimating vertically compensates for the variations of Be length by varying the spacing between blades, so that the transmission of high-energy neutrons is spatially uniform across the filter, as shown in Fig. 4. This corresponds approximately to wedges that are 12 cm long and 8 mm thick at the bottom of the filter, and 18 cm long and 5 cm thick at the top. The simulated transmission of high energy neutrons through the proposed filter is about 10^{-4}, which is one order of magnitude better than the simu-

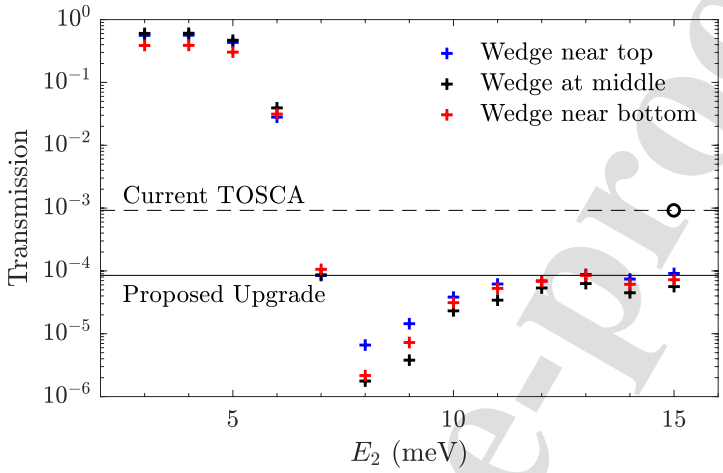

Figure 4: Performance of three beryllium wedges near the top (y = 0.6 m in Fig. 3), middle (y = 0.5 m), and bottom (y = 0.4 m) of the proposed filter. The transmission of high-energy neutrons ($E_2 > 7$ meV) is lower than $8.5 \cdot 10^{-5}$, which is marked by a full line. The transmission of the current filter on TOSCA is calculated to be $9.2 \cdot 10^{-4}$, which is marked by a dashed line. As the incident beam divergence is approximated in this simulation, the transmission of neutrons with $E_2 \leq 5$ meV is inaccurate.

lated performance of the current filter of about 10^{-3}. Despite its complex geometry and the close proximity between neutron absorbing blades at the bottom of the filter, the transmission of low-energy neutrons is 78%, which is a gain by a factor of 1.63 over the transmission of the current filter.

The detector system

The requirements for the detector system are high efficiency (∼90%), a position sensitive resolution of 5–8 mm to resolve the variations of path lengths and secondary TOFs, to be as thin as possible to minimise the distance from the sample plane, and to have the best possible intrinsic time

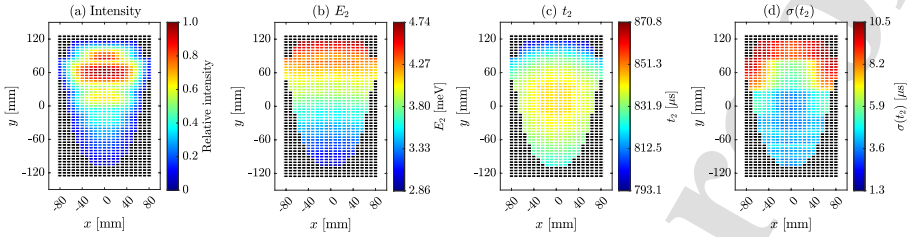

Figure 5: Simulated profiles on the detector in the form of spatial distributions, where each detector pixel is represented by a rectangle and is colour coded depending on the monitored property. (a) Intensities. (b) Means of the distributions of final energies E_2. (c,d) Means and standard deviations of the distributions of secondary TOF t_2. Note the shadows cast on the detector by the neutron absorbing blades of the Be filter.

resolution so that the spectral resolution at high energy transfer is not degraded. Note that this last requirement is motivated by the evaluation of the resolution of the current TOSCA instrument [17], in which we have shown that the intrinsic time resolution of the squashed detectors currently installed on TOSCA is the main contribution to the secondary TOF uncertainties.

A practical solution is to use a single row of ⌀ 8 mm PSD gas tubes with a ^{3}He pressure of 20 bar, which achieves all of these requirements. Crucially, state-of-the-art detectors have an intrinsic time resolution as low as 1 μs, compared to a value estimated in the range 8–10 μs for the current detectors [17]. The average efficiency is estimated to be 89%, which is a gain of 1.10 over the 81% efficiency of the current detector system. About 20 tubes with length of 25 cm are required per detector bank to capture the entire image, for a total of 280 tubes.

The proposed upgrade

The proposed upgrade of the TOSCA secondary spectrometer consists of a staggered assembly of 14 analyser modules (Fig. 1(b)), large, curved, image-focusing PG analysers (Fig. 2), cryo-cooled beryllium filters with a built-in vertical collimation and spatially-uniform filtering performance (Fig. 3–4) and arrays of high-pressure ^{3}He PSD tubes.

The total gain factor of the proposed upgrade over the current instrument, which is obtained by comparing the simulated intensities at the detector for equivalent simulations, is 11.52. Besides the gain from the improved filter transmission (1.63) and improved detector efficiency (1.10), the remaining gain originates from the increased solid angle (6.12; down from 6.3 when including gaps between PG tiles and gaps between analyser banks), and a factor 1.05 which comes from the detector of the current TOSCA being too small in height to capture the entire image. This total gain of 11.52 is independent of the energy transfer and has an associated spectral resolution at $\hbar\omega = 150$ meV of 1.07% of the incident energy.

The simulated beam profiles measured on each pixel of the detector are reported in Fig. 5. The image on the detector is 16 cm wide and 23 cm tall (Fig. 5(a)). The neutron final energies E_2 range from 2.9 meV at the bottom of the detector to 4.7 meV at the top (Fig. 5(b)), with typical uncertainties per pixel $\sigma(E_2) < 0.15$ meV. Despite the radial gradient in secondary TOF t_2 (Fig. 5(c)), the uncertainties in t_2 are small, $\sigma(t_2) \leq 10.5$ μs, with most pixels having $\sigma(t_2) \leq 6$ μs (Fig. 5(d)). Note that these values of $\sigma(t_2)$ include the contributions from the sample, tile and detector thicknesses.

As the distribution of $\sigma(t_2)$ is inhomogeneous, with lower uncertainties

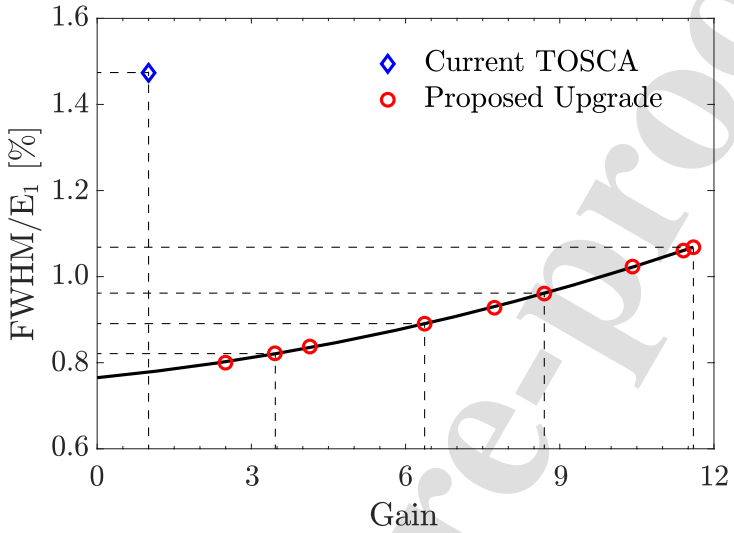

Figure 6: Resolution versus gain for the proposed upgrade for various masks (red circles) and current TOSCA (blue diamond). The resolution is for $\hbar\omega = 150$ meV. The trend of the trade-off between gain and resolution is shown by the thick black line.

at the centre and lower half of the image, so is the spectral resolution at high energy transfer where $\sigma(t_2)$ is the main contribution. This provides an opportunity, in the data reduction process, to mask the detector pixels with the worst resolution, in order to flexibly trade gain for resolution. This is particularly useful for experiments in which the line widths of spectral bands are of interest, or experiments where spectral features are strongly overlapping. This is illustrated in Fig. 6, which shows that the resolution can be improved from 1.1% down to 0.8% of the incident energy, at the price of a factor 4 in intensity, which is still an improvement of factor 3 in gain over the current TOSCA. Note that, as this feature is part of the data reduction, it can be flexibly adjusted after the experiment depending on the

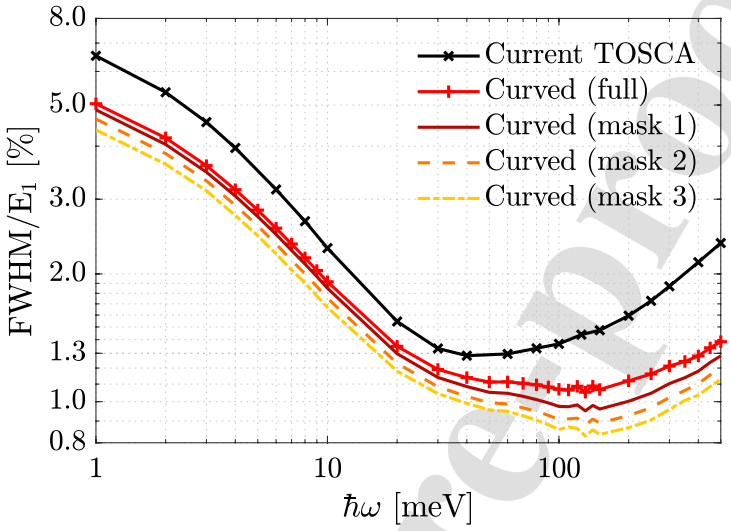

Figure 7: Comparison of the resolution as FWHM/E_1 in % between the current TOSCA (black line and crosses) and the proposed curved analyser, using the entire detector (red line and pluses), and using masks to trade-off gain and resolution in the data reduction (full, dashed, and dashed dotted lines).

requirements of the data analysis. Our experience with TOSCA is that we expect most experiments will use the maximum gain scenario and that only a very limited number of experiments will require the improved resolution.

Finally, we show in Fig. 7 the energy dependence of the spectral resolution for the current TOSCA and the proposed upgrade, using the entire detector bank and three different masks in the data reduction. The spectral resolution of the proposed upgrade improves over the current TOSCA for all energy transfers. At the elastic line and at low energy transfers, the improved resolution is due to the reduced relative uncertainties in secondary flight paths, thanks to the near-elliptical curvature of the PG analysers and

the increased secondary flight path. At high energy transfers, the improved resolution is a result of the significantly enhanced time resolution of the proposed PSDs over the current detectors, and of the design of the curved PG analyser that minimises its contribution to the uncertainties in secondary time-of-flights.

For comparison, the plateau of the spectral resolution at high energy transfer is estimated at $\leq$1.5% of the incident energy for VISION, and $\leq$1.8% and $\leq$2.5% for LAGRANGE [29], for the Cu331 and Cu220 monochromators, respectively. The predicted resolution plateaus of VESPA are $\leq$2.0% and $\leq$0.8% of the incident energy [13], for the low and high-resolution settings, respectively. With a predicted resolution of $\leq$1.1% that can be improved to $\leq$0.8%, which is achieved for a large sample of $40 \times 40 \times 1$ mm^3, and with its tenfold increase in detected intensity, the TOSCA upgrade will put the instrument performance on par with spectrometers at much brighter sources.

Conclusions

We have presented an overview of the TOSCA secondary spectrometer upgrade project, planned as part of the Endeavour instrument upgrade program at the ISIS Neutron and Muon Source, U.K. The proposed upgrade will see the replacement of the entire secondary spectrometer with the installation of 14 new analyser modules in a staggered assembly. The curved image-focusing PG analyser will cover an extremely large solid angle of 6.12 steradians which, together with the improved transmission of analysed neutrons through the beryllium filter, and improved neutron capture efficiency of the detector system, leads to a predicted gain in detected intensity of 11.5

over the current TOSCA, independent of energy transfer. This is achieved while improving the signal-to-noise ratio by better filtering of high energy neutrons by the beryllium filter and improving the spectral resolution over the entire range of energy transfer of the instrument. The predicted resolution in the fingerprint region is $\leq$1.1% of the incident energy, which can be further improved to $\leq$0.8% by flexibly trading gain for resolution by using masks in the data reduction process. The overall performance gain in detected intensity, SNR and spectral resolution will enable TOSCA to tackle new and challenging experiments and ensure that it remains highly competitive in the international landscape of neutron chemical spectrometers.

Acknowledgements

This work was supported by the Science and Technology Facilities Council (STFC). The authors thank the NMIDG group at the ISIS Facility for organising the review of the project, and A. Ivanov (ILL), D. Colognesi (CNR), L. Daemen (SNS) and A. J. Ramirez-Cuesta (SNS) for participating in the review and for their helpful comments.

References

[1] L. Lin, M. Fan, A. M. Sheveleva, X. Han, Z. Tang, J. H. Carter, I. da Silva, C. M. A. Parlett, F. Tuna, E. J. L. McInnes, G. Sastre, S. Rudić, H. Cavaye, S. F. Parker, Y. Cheng, L. L. Daemen, A. J. Ramirez-Cuesta, M. P. Attfield, Y. Liu, C. C. Tang, B. Han, S. Yang, Control of zeolite microenvironment for propene synthesis from

methanol, Nat. Commun. 12 (2021) 822. doi:10.1038/s41467-021-21062-1.

[2] L. Lin, A. M. Sheveleva, I. da Silva, C. M. A. Parlett, Z. Tang, Y. Liu, M. Fan, X. Han, J. H. Carter, F. Tuna, E. J. L. McInnes, Y. Cheng, L. L. Daemen, S. Rudić, A. J. Ramirez-Cuesta, C. C. Tang, S. Yang, Quantitative production of butenes from biomass-derived γ-valerolactone catalysed by hetero-atomic MFI zeolite, Nat. Mater. 19 (2020) 86–93. doi:10.1038/s41563-019-0562-6.

[3] L. Guo, M. Savage, J. H. Carter, X. Han, I. da Silva, P. Manuel, S. Rudić, C. C. Tang, S. Yang, M. Schröder, Direct visualization of supramolecular binding and separation of light hydrocarbons in MFM-300(In), Chem. Mater. 34 (2022) 5698–5705. doi:10.1021/acs.chemmater.2c01097.

[4] Y. Ma, W. Lu, X. Han, Y. Chen, I. da Silva, D. Lee, A. M. Sheveleva, Z. Wang, J. Li, W. Li, M. Fan, S. Xu, F. Tuna, E. J. L. McInnes, Y. Cheng, S. Rudić, P. Manuel, M. D. Frogley, A. J. Ramirez-Cuesta, M. Schröder, S. Yang, Direct observation of ammonia storage in UiO-66 incorporating Cu(II) binding sites, J. Am. Chem. Soc. 144 (2022) 8624–8632. doi:10.1021/jacs.2c00952.

[5] M. Tian, M. J. Lennox, A. J. O'Malley, A. J. Porter, B. Krüner, S. Rudić, T. J. Mays, T. Düren, V. Presser, L. R. Terry, S. Rols, Y. Fang, Z. Dong, S. Rochat, V. P. Ting, Effect of pore geometry on ultra-densified hydrogen in microporous carbons, Carbon 173 (2021) 968–979. doi:10.1016/j.carbon.2020.11.063.

[6] L. Mazzei, F. Piccinelli, M. Bettinelli, S. F. Parker, M. Karlsson, The effect of cation substitution on the local coordination of protons in $Ba_2In_{1.85}M_{0.15}O_6H_2$ (M = In, Ga, Sc and Y), Solid State Ion. 365 (2021) 115624. doi:10.1016/j.ssi.2021.115624.

[7] C. Eklöf-Österberg, L. Mazzei, E. J. Granhed, G. Wahnström, R. Nedumkandathil, U. Häussermann, A. Jaworski, A. J. Pell, S. F. Parker, N. H. Jalarvo, L. Börjesson, M. Karlsson, The role of oxygen vacancies on the vibrational motions of hydride ions in the oxyhydride of barium titanate, J. Mater. Chem. A 8 (2020) 6360–6371. doi:10.1039/C9TA11912D.

[8] M. M. Nolasco, C. F. Araujo, S. Thiyagarajan, S. Rudić, P. D. Vaz, A. J. D. Silvestre, P. J. A. Ribeiro-Claro, A. F. Sousa, Asymmetric monomer, amorphous polymer? Structure–property relationships in 2,4-FDCA and 2,4-PEF, Macromolecules 53 (2020) 1380–1387. doi:10.1021/acs.macromol.9b02449.

[9] M. P. M. Marques, A. L. M. Batista de Carvalho, A. P. Mamede, A. Dopplapudi, S. Rudić, M. Tyagi, V. García Sakai, L. A. E. Batista de Carvalho, A new look into the mode of action of metal-based anticancer drugs, Molecules 25 (2020) 246. doi:10.3390/molecules25020246.

[10] B. E. Souza, S. Rudić, K. Titov, A. S. Babal, J. D. Taylor, J.-C. Tan, Guest–host interactions of nanoconfined anti-cancer drug in metal–organic framework exposed by terahertz dynamics, Chem. Commun. 55 (2019) 3868–3871. doi:10.1039/C8CC10089F.

[11] M. L. Martins, A. B. Dinitzen, E. Mamontov, S. Rudić, J. E. M. Pereira, R. Hartmann-Petersen, K. W. Herwig, H. N. Bordallo, Water dynamics in MCF-7 breast cancer cells: a neutron scattering descriptive study, Sci. Rep. 9 (2019) 8704. doi:10.1038/s41598-019-45056-8.

[12] P. A. Seeger, L. L. Daemen, J. Z. Larese, Resolution of VISION, a crystal-analyzer spectrometer, Nucl. Instrum. Methods Phys. Res., Sect. A 604 (2009) 719–728. doi:10.1016/j.nima.2009.03.204.

[13] M. Zanetti, S. Bellissima, L. del Rosso, F. Masi, M. Chowdhury, A. De Bonis, L. Di Fresco, C. Scatigno, J. Armstrong, S. Rudić, S. Parker, M. Hartl, D. Colognesi, R. Senesi, C. Andreani, G. Gorini, F. Fernandez-Alonso, Neutronic developments on TOSCA and VESPA: Progress to date, Physica B: Condensed Matter 562 (2019) 107–111. doi:10.1016/j.physb.2018.12.034.

[14] K. Andersen, D. Argyriou, A. Jackson, J. Houston, P. Henry, P. Deen, R. Toft-Petersen, P. Beran, M. Strobl, T. Arnold, H. Wacklin-Knecht, N. Tsapatsaris, E. Oksanen, R. Woracek, W. Schweika, D. Mannix, A. Hiess, S. Kennedy, O. Kirstein, S. Petersson Årsköld, J. Taylor, M. Hagen, G. Laszlo, K. Kanaki, F. Piscitelli, A. Khaplanov, I. Stefanescu, T. Kittelmann, D. Pfeiffer, R. Hall-Wilton, C. Lopez, G. Aprigliano, L. Whitelegg, F. Moreira, M. Olsson, H. Bordallo, D. Martín-Rodríguez, H. Schneider, M. Sharp, M. Hartl, G. Nagy, S. Ansell, S. Pullen, A. Vickery, A. Fedrigo, F. Mezei, M. Arai, R. Heenan, W. Halcrow, D. Turner, D. Raspino, A. Orszulik, J. Cooper, N. Webb, P. Galsworthy, J. Nightingale, S. Lan-

gridge, J. Elmer, H. Frielinghaus, R. Hanslik, A. Gussen, S. Jaksch, R. Engels, T. Kozielewski, S. Butterweck, M. Feygenson, P. Harbott, A. Poqué, A. Schwaab, K. Lieutenant, N. Violini, J. Voigt, T. Brückel, M. Koenen, H. Kämmerling, E. Babcock, Z. Salhi, A. Wischnewski, A. Heynen, S. Désert, J. Jestin, F. Porcher, X. Fabrèges, G. Fabrèges, B. Annighöfer, S. Klimko, T. Dupont, T. Robillard, A. Goukassov, S. Longeville, C. Alba-Simionesco, P. Bourges, J. Guyon Le Bouffy, P. Lavie, S. Rodrigues, E. Calzada, M. Lerche, B. Schillinger, P. Schmakat, M. Schulz, M. Seifert, W. Lohstroh, W. Petry, J. Neuhaus, L. Loaiza, A. Tartaglione, A. Glavic, S. Schütz, J. Stahn, E. Lehmann, M. Morgano, J. Schefer, U. Filges, C. Klauser, C. Niedermayer, J. Fenske, G. Nowak, M. Rouijaa, D. Siemers, R. Kiehn, M. Müller, H. Carlsen, L. Udby, K. Lefmann, J. Birk, S. Holm-Dahlin, M. Bertelsen, U. B. Hansen, M. Olsen, M. Christensen, K. Iversen, N. Christensen, H. Rønnow, P. Freeman, B. Hauback, R. Kolevatov, I. Llamas-Jansa, A. Orecchini, F. Sacchetti, C. Petrillo, A. Paciaroni, P. Tozzi, M. Zanatta, P. Luna, I. Herranz, O. del Moral, M. Huerta, M. Magán, M. Mosconi, E. Abad, J. Aguilar, S. Stepanyan, G. Bakedano, R. Vivanco, I. Bustinduy, F. Sordo, J. Martínez, R. Lechner, F. Villacorta, J. Šaroun, P. Lukáš, M. Markó, M. Zanetti, S. Bellissima, L. del Rosso, F. Masi, C. Bovo, M. Chowdhury, A. De Bonis, L. Di Fresco, C. Scatigno, S. Parker, F. Fernandez-Alonso, D. Colognesi, R. Senesi, C. Andreani, G. Gorini, G. Scionti, A. Schreyer, The instrument suite of the European Spallation Source, Nucl. Instrum. Methods Phys. Res., Sect. A 957 (2020) 163402. doi:10.1016/j.nima.2020.163402.

[15] S. F. Parker, F. Fernandez-Alonso, A. J. Ramirez-Cuesta, J. Tomkinson, S. Rudić, R. S. Pinna, G. Gorini, J. Fernández Castañon, Recent and future developments on TOSCA at ISIS, J. Phys. Conf. Ser. 554 (2014) 012003. doi:10.1088/1742-6596/554/1/012003.

[16] P. C. H. Mitchell, S. F. Parker, A. J. Ramirez-Cuesta, J. Tomkinson, Vibrational Spectroscopy with Neutrons, World Scientific, London, 2005, Ch. 3, Instrumentation and Experimental Methods, pp. 67–136. doi:10.1142/5628.

[17] A. Perrichon, On the spectral resolution of the broad-band indirect-geometry time-of-flight neutron spectrometer TOSCA, Nucl. Instrum. Methods Phys. Res., Sect. A 1041 (2022) 167401. doi:10.1016/j.nima.2022.167401.

[18] A. Perrichon, TOSCA Secondary Spectrometer Upgrade. Part I – Analytical and Monte Carlo Study of the Spectral Resolution of TOSCA, STFC RAL Technical Report RAL-TR-2021-002, DOI:10.5286/raltr.2021002 (2021).

[19] R. S. Pinna, S. Rudić, S. F. Parker, J. Armstrong, M. Zanetti, G. Škoro, S. P. Waller, D. Zacek, C. A. Smith, M. J. Capstick, D. J. McPhail, D. E. Pooley, G. D. Howells, G. Gorini, F. Fernandez-Alonso, The neutron guide upgrade of the TOSCA spectrometer, Nucl. Instrum. Methods Phys. Res., Sect. A 896 (2018) 68–74. doi:10.1016/j.nima.2018.04.009.

[20] R. S. Pinna, S. Rudić, S. F. Parker, G. Gorini, F. Fernandez-Alonso, Monte carlo simulations of the TOSCA spectrometer: Assessment of

current performance and future upgrades, EPJ Web Conf. 83 (2015) 03013. doi:10.1051/epjconf/20158303013.

[21] M. Zanetti, F. Masi, S. Rudić, J. Armstrong, S. F. Parker, F. Fernandez-Alonso, G. Gorini, Crystal Analyzers for Indirect-Geometry Broadband Neutron Spectrometers: Adding Reality to Idealized Design, J. Synch. Investig. 14 (2020) S242–S250. doi:10.1134/S1027451020070526.

[22] R. S. Pinna, S. Rudić, M. Zanetti, D. Zacek, S. F. Parker, G. Gorini, F. Fernandez-Alonso, Monte Carlo Simulations for the TOSCA Secondary Spectrometer Upgrade, STFC RAL Technical Report RAL-TR-2017-013, DOI:10.5286/raltr.2017013 (2017).

[23] C. Scatigno, M. Zanetti, S. Rudić, R. Senesi, C. Andreani, G. Gorini, F. Fernandez-Alonso, Hydrogen Detection Limits and Instrument Sensitivity of High-Resolution Broadband Neutron Spectrometers, Anal. Chem. 94 (2022) 5023–5028. doi:10.1021/acs.analchem.1c04949.

[24] J. Armstrong, S. Banerjee, V. Schünemann, J. A. Wolny, P. J. Sadler, Vibrational motions make significant contributions to sequential methyl C–H activations in an organometallic complex, J. Phys. Chem. Lett. 12 (2021) 658–662. doi:10.1021/acs.jpclett.0c03292.

[25] F. Webb, The leakage of thermal neutrons through beryllium filters, Nucl. Instrum. Methods 69 (1969) 325–329. doi:10.1016/0029-554X(69)90432-7.

[26] K. Lefmann, K. Nielsen, McStas, a general software package for

neutron ray-tracing simulations, Neutron News 10 (1999) 20–23. doi:10.1080/10448639908233684.

[27] P. Willendrup, E. Farhi, K. Lefmann, McStas 1.7 – a new version of the flexible Monte Carlo neutron scattering package, Physica B: Condensed Matter 350 (2004) E735–E737. doi:10.1016/j.physb.2004.03.193.

[28] P. Willendrup, K. Lefmann, McStas (ii): An overview of components, their use, and advice for user contributions, J. Neutron Res. 23 (2021) 7–27. doi:10.3233/JNR-200186.

[29] A. Ivanov, M. Jimenéz-Ruiz, J. Kulda, IN1-LAGRANGE – the new ILL instrument to explore vibration dynamics of complex materials, J. Phys. Conf. Ser. 554 (2014) 012001. doi:10.1088/1742-6596/554/1/012001.

Declaration of interests

☒ The authors declare that they have no known competing financial interests or personal relationships that could have appeared to influence the work reported in this paper.

☐ The authors declare the following financial interests/personal relationships which may be considered as potential competing interests: